Paper ID AM-SP1290

Combating Ground Reflection for Wireless Sensors

Ashutosh Tadkase[1], **Nagarjun Srinivasan**[2], and **Bob Iannucci**[2]
1. Carnegie Mellon University, Department of Electrical and Computer Engineering
NASA Ames Research Park, Moffett Field, CA 94035 USA
+1 781 888 1790 – ashutosh.tadkase@sv.cmu.edu
2. Carnegie Mellon University, Department of Electrical and Computer Engineering, USA

Abstract:
Low-power sensing and communication technologies have evolved to the point where it is feasible to install intelligent, wirelessly-connected sensors pervasively on roadways to enable precise, real-time monitoring of traffic flows. Efficient operation of the sensing, computing and communications subsystems in these devices offers the possibility of battery lifetimes comparable to replacement cycles for normal raised pavement markers, making install-and-forget sensing a practical reality. But such unobtrusive mounting on the road surface brings with it an inherent problem. Data signals sent from the wireless devices in these sensors suffer from the effect of ground reflection which distort the antenna's pattern. We explore this fundamental problem and its possible solutions from first principles. We offer an approach for antenna / enclosure co-design that yields a 6 dB gain improvement over a simple dipole antenna.
KEYWORDS: Ground reflection, wireless sensors, antennas

I. Introduction

Technology advances over the last two decades in sensing, computing and communications technologies have enabled the possibility of real-time, fine-grained (in space and time) measurements of traffic flows. In our companion paper [1], we introduce the concept of the *crowdsourced smart city* as an approach for incrementally introducing sensors and data communications networks into cities in ways that align well with typical city practices and for the purpose of kick-starting the process of gathering, curating, and making sense of the substantial information produced in cities each day. A key technology enabler is the low-power wide-area network (LP-WAN) that aids these small devices in achieving installed lifetimes measured in years.

We have developed a sensing device suitable for many applications in the smart city, and together with our research partners, we are installing and evaluating these sensors and companion LP-WAN networks for a traffic calming application. Our sensor, the CMU TrafficDot (Figure 1), is a raised pavement marker (RPM) containing a sophisticated magnetometer-based sensing system coupled with signal processing capabilities and an LP-WAN transceiver. Our studies [1], [2] and those of others reveal the benefits of LP-WAN networks for smart city applications.

We have augmented our devices and network with a set of web-based tools that offer city officials real-time traffic visualizations and the ability to analyze flows over days, weeks, or longer. Among other applications, the TrafficDot with its fine-grained, always-on monitoring capabilities allows quantitative A-B comparisons of traffic calming interventions. Battery-based wireless operation enables rapid deployment and re-deployment.

The TrafficDot uses a precision magnetometer to sense the passage of cars and trucks. With signal processing, it is possible not only to provide geo-referenced, time-stamped counts but also to estimate speeds and vehicle types.

But our sensor and, in fact, similar smart-city sensors of various types suffer from a common and pernicious problem. By mounting the device directly on the road surface, the performance of the inbuilt LP-WAN antenna is compromised. The road surface serves as a reflector, and these reflections work against aiming precious

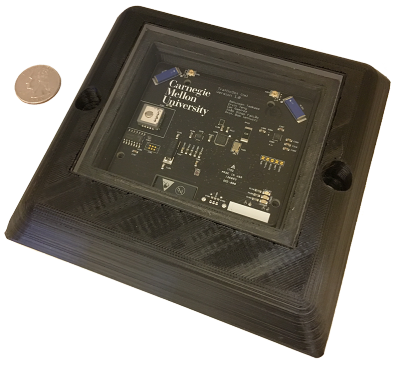

Fig. 1: CMU's TrafficDot – an intelligent RPM for counting vehicles and measuring speed.

signal energy toward the LP-WAN gateway. A typical antenna pattern is shown in Figure 2. Antenna engineers euphemistically call this the "cloud burner" pattern as the majority of signal power goes straight up, only to be dissipated as heat. Because we seek to cover distances of miles with a single gateway, we require good antenna performance at low elevation angles (Figure 4).

In this paper, we explore the problem of ground reflection for pavement-mounted sensors and identify techniques where some measure of horizontal directivity can be restored. This, then, can form the basis for future work in adaptive beamforming toward the gateway. Section II presents the ground reflection challenge for roadway-mounted sensors more formally. In Section IV, we explore the co-design of enclosure and antenna that might serve to overcome pathological antenna performance. Section V gives the results of our studies. We then conclude with recommendations for future work.

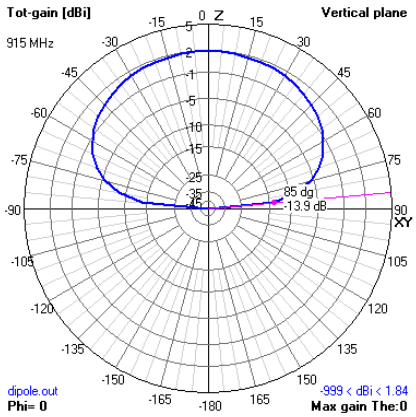

Fig. 2: Elevation pattern of a 915 MHz half-wave dipole suspended 0.1λ above real ground. The antenna's maximum gain is straight up, but the gain at an elevation angle of $5°$ (indicated) from the horizontal is -13.9 dB, representing significant loss.

Contributions: This work presents a study of ground-mounted, radio-equipped sensors such as one will find in the smart city. This study provides

- An analytical approach for quantifying antenna losses as they relate to pavement-mounted sensors for smart cities, and
- A methodology for co-designing the antenna and the roadway-mounted enclosure to optimize gain without sacrificing space or compromising mechanical performance.

II. Analytical Approach

The CMU TrafficDot is representative of a broad class of smart city sensing devices. Each will have one or more transducers, a small processor, some storage, a battery, a radio, and an antenna subsystem. Robustness of the physical enclosure is a must. External antennas, particularly ones that are obtrusive, are impractical in many situations. So, in general, we assume the physical constraints of the smart city compel us to consider internal antennas. With the positioning of such smart city sensors on buildings, other fixtures, or the ground, we have the compound problem of physically compromised antennas and the effect of a proximate ground plane.

A. Physical Constraints of the TrafficDot

Smart city sensors will doubtless come in a variety of sizes and shapes. In our case, and presumably in other cases, dimensions will be constrained by considerations other than the degree to which the electronics can be minimized. The basic ability to transmit data over a noisy wireless channel on an ongoing basis will necessitate a substantial power source. If we would seek to power the device with a solar cell, there will be a size limit below which the harvested power will be insufficient to provide the radio connectivity that the overall application needs (resulting in either distance limits, information latency limits, or both). Energy densities of commercial batteries and desired sensor life-times similarly constrain sensor volume. As we shall explore, the choice of transmitting frequency will further impose size constraints driven by the wavelength of the signal.

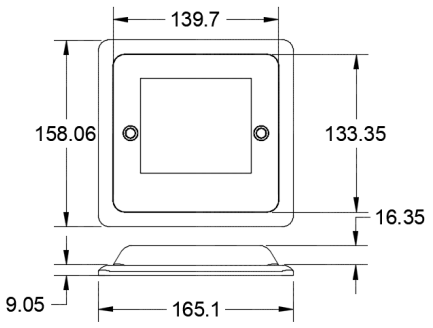

Fig. 3: Dimensions of the TrafficDot (mm)

The CMU TrafficDot is designed to operate in the US Industrial/Scientific/Medical band between 902 and 928 MHz. The lifetime specification is five years, and we assume the amount of energy that can be harvested via solar is not so reliable as to be a basis for operation. Instead, our sensor houses a single AA lithium thionyl chloride ($LiSOCl_2$) primary cell. The housing's dimensions, as shown in Figure 3, reflect these constraints as well as the need to meet mechanical strength properties comparable to other RPMs. The space budget for the antenna subsystem is, therefore, highly constrained. We anticipate the desire to further shrink sensors so as to better meet other smart city applications. We therefore take the dimensions in the figure as an upper bound.

B. Physical Layout in the Smart City

LP-WAN networks such as LoRa from Semtech [3] use *gateways* mounted on poles, buildings or other permanent structures to communicate to wireless devices in proximity. The economics of an LP-WAN network, as in other wireless networks, are based on minimizing the number of such gateways (each brings costs associated with equipment, installation, maintenance, and the provisioning of communications from the gateway to the larger internet–called *backhaul*) subject to coverage and capacity constraints. A possible arrangement is shown in Figure 4 where the gateway is mounted on the roof of a building and the sensors–in our case, TrafficDots–are affixed to the streets surrounding the building. To understand the economics, we must relate radio frequency (RF) performance of the sensors to their distance from the serving gateway(s) based on environmental conditions as well as factors attributable to the sensor's antenna.

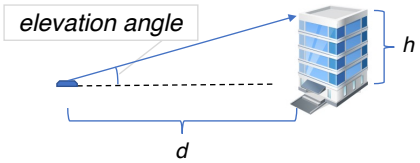

Fig. 4: Sensors in the smart city will communicate with one or more gateways mounted on city structures. The area that a single gateway can serve depends on the environment and on the properties of the sensor and its antenna subsystem. Optimal orientation of the sensor antenna toward the gateways varies in three dimensions. Antenna performance at the *elevation angle* is especially important.

C. Link Budget

RF engineering approaches this challenge by modeling how power levels vary from the transmitter to the receiver based on separable effects. The transmitter's power output level and the receiver's sensitivity to weak signals represent the bounds, and elements along the path contribute gains and losses. The accounting for the gains and losses represents the wireless *link budget*. In plain terms, the power level at the receiver is the power from the transmitter plus gains and minus losses. The area a gateway can serve is exactly that area where this power level is above the minimum level set by the receiver's sensitivity. Figure 5 captures the essential elements of link budget, summarized by Equation 1:

$$P_{rx} = P_{tx} - P_{txcbl} + P_{txant} - PL + P_{rxant} - P_{rxcbl} \quad (1)$$

where P_{tx} is the given output power of the transmitter (capped by regulation and/or by battery lifetime considerations), P_{txcbl} and P_{rxcbl} are losses attributable to the cables at the transmitter and receiver, P_{txant} and P_{rxant} are the gains (or losses) of the transmit and receive antennas, and PL is the path loss between the antennas. P_{rx} is the resulting power available at the input to the receiver. The domain that can be covered, then, is the set of all sensors for which $P_{rx} > P_{rxmin}$. While in practice the contour of this domain will be irregular due to environmental factors, we can approximate it as the circle of radius r in which all sensors meet the $P_{rx} > P_{rxmin}$ condition.

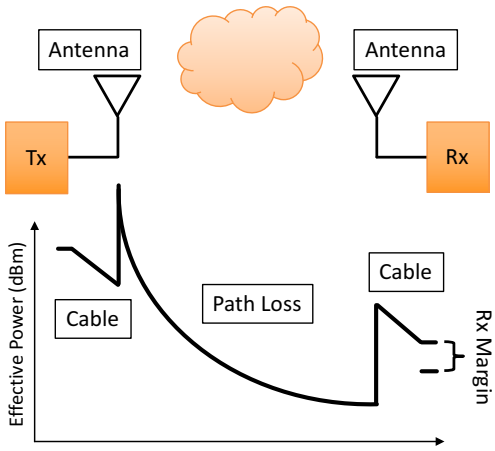

Fig. 5: Signal strength at the receiver is a function of transmitter signal strength, cable losses, antenna gains (or losses), and free space path loss. With power being capped by regulation and receive sensitivity set by technology, maximizing distance is done by optimizing the antenna subsystems.

For the operating frequencies in question and the design parameters of typical sensors and gateways, the cable losses can be ignored ($P_{txcbl} = P_{rxcbl} = 0$). Gateway antenna gain is both well-tabulated in data sheets and realizable in practice with proper mounting and attention to environmental conditions. While not always the case, the typical LP-WAN gateway antenna will be chosen to provide an omni-directional pattern in azimuth and a narrow beamwidth in elevation. Gains of 8-10 dBi (gain relative to a true isotropic antenna) are typical.

Path loss PL is complex to characterize, and modeling for realistic cases is beyond the scope of this study. So-called free-space path loss (FSPL) gives a rough estimate based on frequency (f) and distance (d) but without any consideration for blockages, multipath propagation and other effects. It is given (in decibels) by Equation 2:

$$FSPL_{dB} = 20log_{10}(\frac{4\pi df}{c}) \tag{2}$$

What remains, then, is the challenge of characterizing and maximizing the gain or loss at the sensor's antenna.[1]

D. Estimating Ground Reflection Effect

Free space path loss is a gross approximation and does not necessarily represent the path loss experienced in the smart city with pavement-mounted sensors. Antennas are systems whose performance is intimately tied to the environment in which they operate. In particular, we must include the effects of the surfaces on which the sensors are mounted (including their material properties) in order to more accurately model path loss. We adopt the two-ray model used by Sommer *et al.* [4]. Refer to Figure 6.

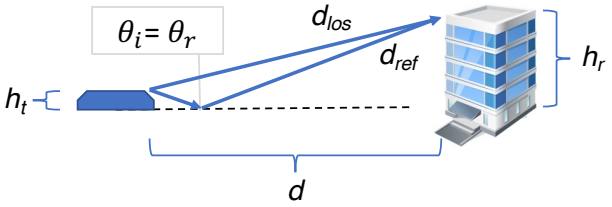

Fig. 6: Two-Ray Propagation Model

In this model, the signal received at gateway is the superposition of two rays: one of which reaches the gateway via line-of-sight and the other via ground reflection. The phase difference between these is given by

$$\varphi = 2\pi(\frac{d_{los} - d_{ref}}{\lambda}) \tag{3}$$

$$d_{los} = \sqrt{d^2 + (h_r - h_t)^2} \tag{4}$$

$$d_{ref} = \sqrt{d^2 + (h_r + h_t)^2} \tag{5}$$

The ground reflection coefficient depends on the angle of incidence (or reflection) θ_i and the relative permittivity of ground ϵ_r. Geometrically,

$$sin\theta_i = (h_t + h_r)/d_{ref} \tag{6}$$

$$cos\theta_i = d/d_{ref} \tag{7}$$

The reflection coefficient for a horizontally polarized antenna[2] is

$$\Gamma(\theta_i) = \frac{sin\theta_i - \sqrt{\epsilon_r - cos^2\theta_i}}{sin\theta_i + \sqrt{\epsilon_r - cos^2\theta_i}} \tag{8}$$

Sommer *et. al* [4] amend Equation 2 with a correction term to account for the (complex) interference as follows:

$$PL_{2ray,dB} = 20log_{10}(\frac{4\pi d}{\lambda}|1 + \Gamma(\theta_i)e^{i\varphi}|^{-1}) \tag{9}$$

For large values of d, $\varphi \to 0$ and we can approximate the path loss as

$$PL_{dB} = 20log_{10}(\frac{4\pi d}{\lambda}|1 + \Gamma(\theta_i)|^{-1}) \tag{10}$$

[1]While the electromagnetic property of *reciprocity* guarantees us that the gains or losses of our two antennas is independent of our choice of which one is serving as the transmitter and which is serving at the receiver, the case of our sensor being the transmitter is by far the more challenging one. With power being constrained at the sensor, but not at the gateway, $P_{txGateway}$ can easily exceed $P_{txSensor}$, making the gateway-transmitting problem easier than the sensor-transmitting problem. In this paper, we focus on the latter.

[2]The low-profile nature of an RPM and the wavelength of operation favor a horizontally-polarized antenna solution. Note that this has implications at the gateway where the traditional solution is an omni-directional (vertical) monopole. A horizontally-polarized antenna at the gateway will not have an omni-directional azimuthal pattern. This deployment consideration is beyond our present scope.

The difference between free space performance and performance in the presence of a ground plane is estimated for a median value of dry concrete's relative permittivity in Figure 7. As the distance from gateway to sensor grows, not only does the free space path loss grow, the additional losses due to the proximity to ground grow. Recognizing that ground proximity losses are inherent to pavement mounted sensors, we turn our attention to ways in which we can design the antenna subsystem for the sensor to minimize losses. We employ simulation tools and models that capture the ground effect.

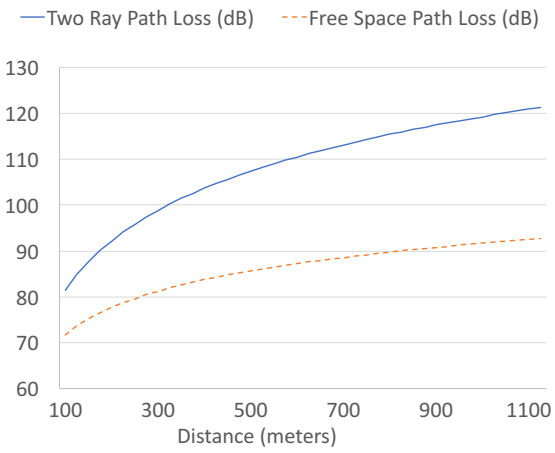

Fig. 7: Two-ray path loss including ground reflection *vs.* free space path loss as a function of distance between gateway and sensor.

E. Antenna Pattern

Specification sheets for antennas are often given for the free-space case which, of course, is not the situation for ground-mounted sensors. Simulation tools such as 4NEC2 [5] and CST Studio [6] model ground effects. We use simulation as a way to compare the performance of different antennas with ground effect, but we acknowledge that actual values of ground effect in a realistic deployment merit further analysis specific to the environment (*e.g.,* concrete *vs.* asphalt road surfaces).

A figure-of-merit that will guide our selection is the antenna's *gain* at a low angle from horizontal such as will be encountered by the sensors most distant from the gateway where we know the losses will be highest. Gain $G(f, \theta, \phi)$ is the result of an antenna's *directivity* and its *efficiency* at a given frequency f and direction (θ horizontally and ϕ vertically). Directivity and gain are reported as the ratio of that antenna's radiation intensity in the given direction to the radiation intensity of an isotropic reference, in decibels (units: dBi).

We use the term *elevation angle* to refer to the *angle from horizontal* to the direct line between sensor and gateway. It is clear that the most distant sensors in level terrain will face elevation angles of a few degrees at best (*e.g.,* with the gateway at 40 meters, TrafficDots beyond 500 meters will face elevation angles less than $5°$). Referring again to Figure 2, the simple dipole antenna performs poorly, with a gain of -13.9 dBi at $5°$ (that's *loss* relative to an isotropic antenna), declining to lower values as the distance increases and the elevation angle is further reduced.

To improve the plight of distant sensors and, thereby, to increase the area covered by each of our LP-WAN smart city gateways, we seek an antenna subsystem for sensors that exhibits better gain at low elevation angles. This could come from an overall "flattening" of the antenna's pattern and/or from some directional bias–focusing, or aiming more power in a particular wedge of the horizontal plane at the expense of others. Note that "flattening" is more desirable. Aiming would necessitate some sort of means in the sensor itself to point the so-formed beam in the direction of the gateway (we can't expect our sensor installers to be antenna aiming experts, after all).

F. Performance Figures-of-Merit

Within the constraints that all candidate antennas must tune the target range of frequencies (in our case, 902-928 MHz with a voltage standing wave ratio (VSWR) $\leq 2.0:1$) and must be able to fit inside the TrafficDot, we will compare alternatives on the basis of gain improvement over the diplole at a low elevation angle (for our purposes, we will use $5°$ from horizontal as the benchmark) as well as their relative radiation efficiencies.

III. Relevant Prior Work

The effect of ground proximity on antennas has been well-studied. Vogler and Noble [7] have characterized the behavior of ground plane on both horizontal and vertical magnetic and electric dipoles. They have shown that, along with frequency and height above ground, the conductivity of the ground material is an important factor, with high ground conductivity being shown to be a desirable characteristic. Miron [8] presented an analytical treatment of ground reflection by using image theory, along with formulae for deriving the radiation patterns of horizontal and vertical dipoles over a ground plane. In their work, Liao and Sarabandi [9] have simulated an entire channel starting

from the transmission antenna to the receiving antenna and have evaluated multiple electrically small antennas for their performance near ground. They have identified the cavity-backed circular slot antenna to be the best performer for low elevation angles.

Multiple antenna elements have been explored beneficially. Roach and Bernhard showed benefit from phased arrays [10]. Vertical stacking has proven effective for increasing directivity by Kramer, Djerfi and Wu [11]. However, the antenna structure presented, which is tuned for a smaller wavelength with a frequency of 5.8 GHz, will not fit in a TrafficDot when scaled for a frequency of 915 MHz. Another structure by Liang, Qi and Jiao [12] shows good performance for the size, but it is still bigger than the TrafficDot.

In order to fit antennas inside the TrafficDot, antenna structures have to be small, or electrically shortened antennas have to be used. The limitations of electrically small antennas have been documented by Wheeler [13], and formulas relating their dimensions to their efficiencies have been documented. Haskou, Collardey and Sharaiha [14] have shown that electrically small arrays can achieve a large directivity, but the radiation efficiency is low. In their paper, Marg, Schon and Jacob [15] presented the effect of sidewalls on the radiation patterns of patch antennas with respect to their beam-width. Also, it has been stated that enclosure walls can be used for beam-forming. This is an interesting result that, in part, motivates our work.

IV. Co-Design Study

Observing that directive antennas combine active and passive elements [16], we study three separate base antenna types. To each one, we add and optimize horizontal and vertical wideband passive reflective elements with the characteristic that *each could conceivably be constructed as part of the mechanical package* of the sensor, and with the objective of attaining a measure of gain. The base antenna types are

- The Modified Folded Dipole (MFD) Pair
- The Moxon Rectangle
- The Microstrip Patch

We describe each in detail, briefly describe our simulation tools, and outline the experimental procedure.

A. The Modified Folded Dipole Pair

Within the given space, a traditional dipole (approximately 0.5λ wide) will not fit. It is possible to fold the dipole, with some loss in performance. The Modified Folded Dipole has been used for space-constrained applications such as RFID tags [17]. The subject of this exploration is a pair of modified folded dipoles, one of which is driven, and the other of which is passive. Being a type of wire antenna, it can be embedded into the lid of a TrafficDot or otherwise made part of the insulted structure of the sensor.

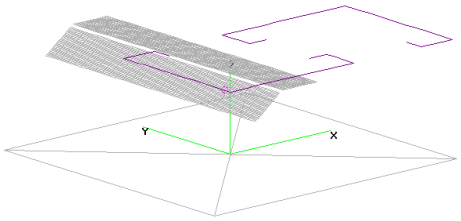

Fig. 8: MFD pair with two reflectors

B. The Moxon Rectangle

The Moxon Rectangle is essentially a folded, two-element Yagi-style antenna. The driven element is a folded dipole and the reflector is likewise folded. As the folded element ends point toward each other, the antenna's overall shape is that of a rectangle. The Moxon exhibits directionality. Our interest in this antenna, like that of the MFD pair, stems from its ability, by virtue of the folds, to fit into the TrafficDot. Figure 9 shows our Moxon wire antenna with two passive reflectors.

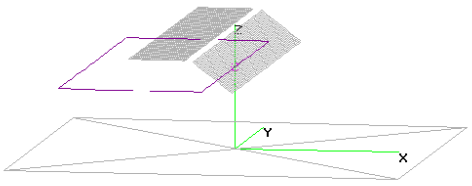

Fig. 9: Moxon Rectangle with two reflectors

C. The Microstrip Patch Antenna

We also studied the Microstrip Patch described by Balanis [16]. A key advantage of certain patch-style antennas is the possibility of integrating them directly onto a printed circuit substrate, simplifying both antenna manufacturing and connection to active circuitry, saving on the cost and (un)reliability of connectors.

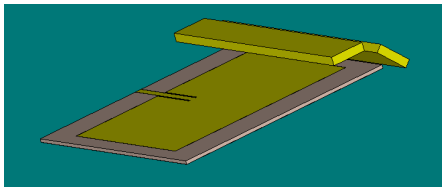

Fig. 10: Microstrip patch with two reflectors

D. Simulation Tools

We selected modeling tools most appropriate for each antenna type. We modeled the wire antennas (Moxon and the MFD) in 4NEC2 [5] and the Microstrip Patch in CST Studio [6]. In 4NEC2, we use surface patches to represent the reflective surfaces

Both tools are capable of modeling the reflective nature of ground to varying degrees. While CST Studio does not support the same ground model as 4NEC2, we are able to approximate the effect of a ground in CST Studio by introducing a 6λx6λx0.125λ concrete slab placed over an infinite ground plane.

E. Experimental Procedure

We evaluate the effectiveness of the three antenna types by following a stepwise constructional procedure for adding reflector elements:

- **Baseline**: Model and simulate the selected antenna at a distance of 0.1λ above the ground plane for a selected frequency (915 MHz in our case).
- **Introduce vertical reflector**: Add a vertical reflector tilted at 45^o near a side of the antenna structure. This side should optimally be the direction in which maximum gain occurs in the azimuthal radiation pattern.
- **Reflector 1 optimization**: Optimize the placement of the reflector with respect to the antenna while keeping both the antenna and the reflector within the physical bounds of the enclosure. The placement is optimized for maximizing the gain while maintaining the VSWR of the antenna below 2.0:1.
- **Introduce horizontal reflector**: Add a horizontal reflector above the antenna structure near the vertical reflector so that it can resemble a part of the top wall of the enclosure.
- **Reflector 2 optimization** Optimize the placement of both reflectors as as before.

To explore the impact of future reductions in the dot's size, we also consider reducing the size of the antenna structures themselves. We select the MFD pair to observe potential reductions in performance and to experiment with means to mitigate these effects. In order to shrink the structure of the MFD, we successively bring the two elements closer, while optimizing the rest of the dimensions for minimum VSWR. These simulations are also conducted with elements placed 0.1λ above the ground plane.

V. Outcome and Analysis

We present azimuth and elevation plots for our three antenna types. In each series of plots, we show the patterns without reflectors and, per our protocol, with the addition of a vertical and then both vertical and horizontal reflectors[3].

A. Simulation Results for the MFD

Figure 11 shows the results for the MFD. Relative to the dipole pattern in Figure 2, we have achieved some beneficial tilt of the elevation pattern, and addition of reflectors yields some further improvement. The two-reflector case improves over the dipole by 4.44 dB (further details in Table II, but the direction is somewhat lopsided–by virtue of the physical asymmetry of the antenna elements.

[3]Notes to the reader: (a) 4NEC2 and CST Studio both reference θ from vertical. As such, our target elevation angle of 5° referenced from horizontal corresponds to $\theta = 85^\circ$. (b) 4NEC2 presents azimuthal plots with the antenna's primary axis pointing ($\theta = 0^\circ$) to the right whereas CST Plus azimuthal plots point upward. (c) Unlike 4NEC2, CST Plus generates plots with a *linear* radial scale.

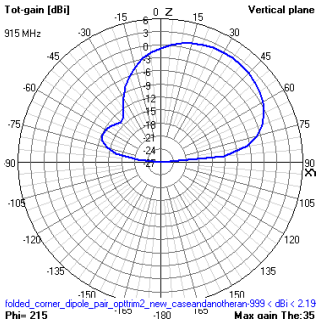

(a) **No reflectors**: Elevation (gain: -12.1 dB)

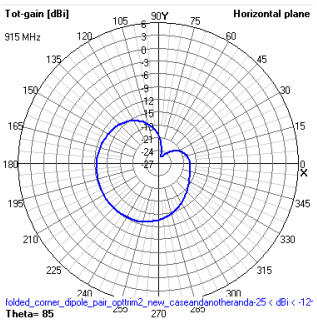

(b) **No reflectors**: Azimuth

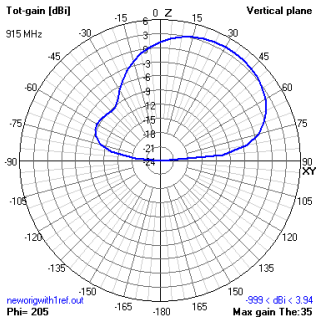

(c) **One reflector**: Elevation (gain: -10.6 dB)

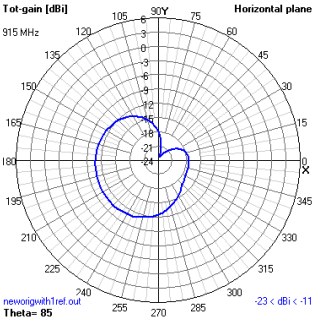

(d) **One reflector**: Azimuth

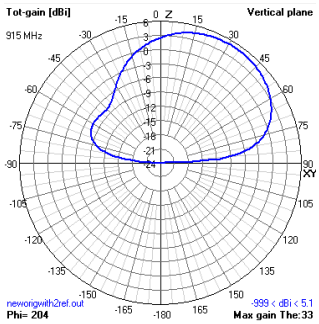

(e) **Two reflectors**: Elevation (gain: -9.46 dB)

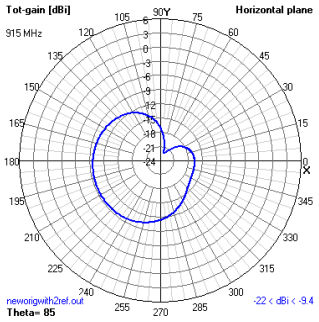

(f) **Two reflectors**: Azimuth

Fig. 11: Radiation patterns showing gain at 5° from horizontal for the MFD pair at 915 MHz

Table I shows the result of exploration of antenna structure on the performance of the MFD pair. Decreasing the separation between the elements decreases the radiation efficiency. Also, it becomes difficult to achieve a low VSWR for smaller wire structures. The gain also decreases from -12.1 dB to -13.1 dB on changing the separation from 11 cm to 7.5 cm. This indicates a trade-off between the size of the antenna structure and the desired performance.

TABLE I: Effect of antenna structure size on performance for MFD pair

Separation	Gain	Radiation Efficiency	VSWR	Impedance
7.5 cm	-13.1 dB	13.16%	1.43	37 + 8.56j
8 cm	-12.8 dB	13.53%	1.31	39.2 + 5.15j
9 cm	-12.3 dB	14.84%	1.16	46.8 + 6.6j
10 cm	-12 dB	17.00%	1.06	50 + 2.99j
11 cm	-12.1 dB	21.61%	1.07	49.9 + 3.1j

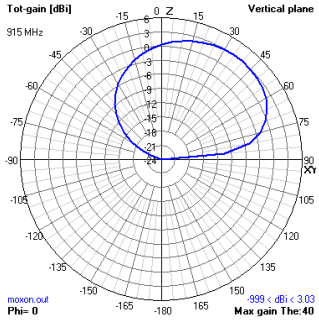

(a) **No reflectors**: Elevation (gain: -10.4 dB)

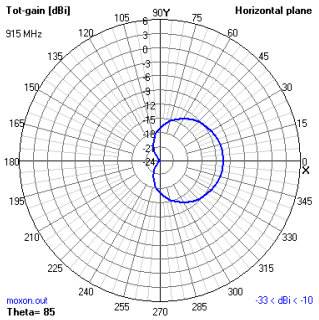

(b) **No reflectors**: Azimuth

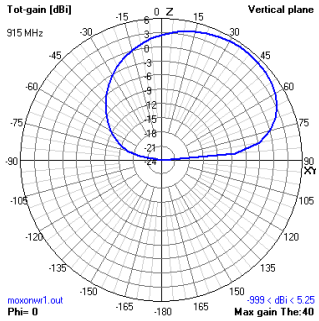

(c) **One reflector**: Elevation (gain: -8.18 dB)

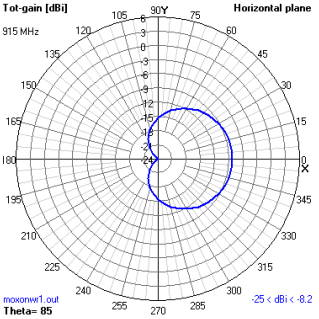

(d) **One reflector**: Azimuth

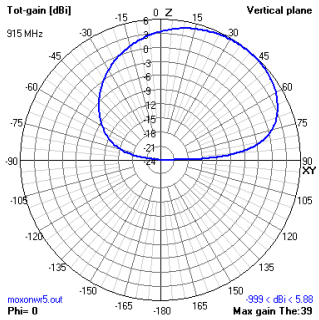

(e) **Two reflectors**: Elevation (gain: -7.62 dB)

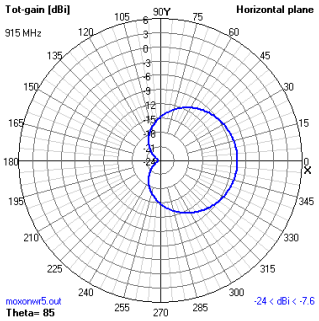

(f) **Two reflectors**: Azimuth

Fig. 12: Radiation patterns showing gain at 5° from horizontal for the Moxon Rectangle at 915 MHz

B. Simulation Results for the Moxon Rectangle

The Moxon's performance overall is quite good. As visible in Figure 12 and as shown in Table II, gain in the forward direction increases as reflectors are added. Net benefit over the dipole is 6.28 dB. Being a wire antenna, physical realization of this geometry in a TrafficDot is space-conserving, and the pattern exhibits good symmetry.

C. Simulation Results for the Microstrip Patch

The Microstrip Patch shows the best gain improvement over the dipole at 6.63 dB with both reflectors added. Manufacturing simplicity (printed circuit) makes this an especially interesting option in that interconnecting wires and the associated losses can be eliminated. Its ratiation efficiency, however, is the worst of the three types at 18-20% with and without reflectors (Table II).

D. Comparison

In all cases, the VSWR was favorable, being below our target of 2.0:1.

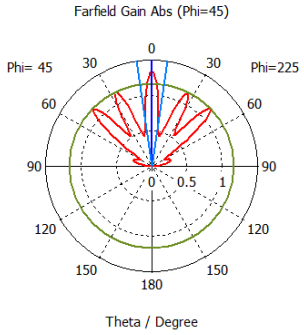

(a) **No reflectors**: Elevation (gain: -9.72 dB)

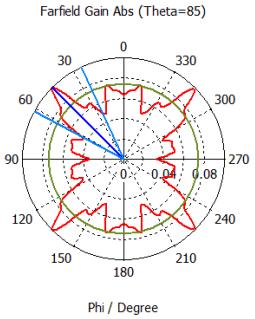

(b) **No reflectors**: Azimuth

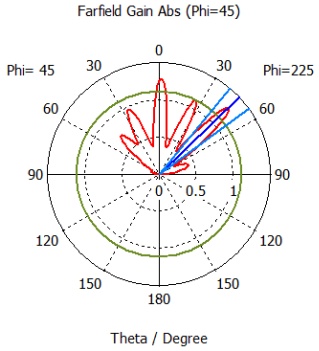

(c) **One reflector**: Elevation (gain: -7.55 dB)

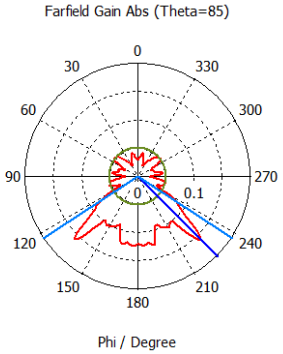

(d) **One reflector**: Azimuth

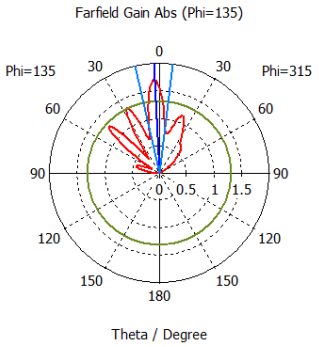

(e) **Two reflectors**: Elevation (gain: -7.27 dB)

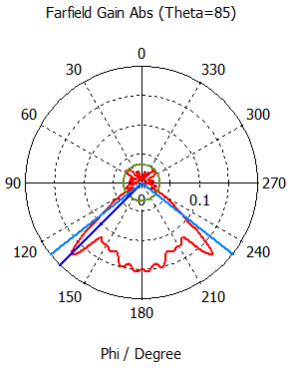

(f) **Two reflectors**: Azimuth

Fig. 13: Radiation patterns showing gain at 5° from horizontal for the Microstrip Patch at 915 MHz

Table II confirms that the addition of reflectors yielded net benefit in gain at the target elevation angle for all three antenna types. The wire antennas (MFD and Moxon) also showed increasing radiation efficiency with the addition of reflectors. The Microstrip patch delivered the best gain improvement at 6.63 dB, with the Moxon a close second at 6.28 dB. But with gains this close, radiation efficiency becomes the determining factor and ultimately favors the Moxon as the best of the three in this study.

The drop in radiation efficiency of the Microstrip bears further investigation. One reason may be the additional capacitance caused by the reflective plates. The surface area of the Microstrip patch is much larger than that of the wire antennas, and this seems to make the effect of capacitance more apparent.

VI. Conclusions and Future Work

We have presented an analytical approach for quantifying antenna losses as they relate to sensors for smart cities. Chief among the important effects is ground reflection, a serious and pervasive issue. Low-profile devices mounted

TABLE II: Effect of reflectors on antenna gain at a 5° elevation angle

Antenna Type	Gain	VSWR	Benefit over dipole	Radiation Efficiency
MFD Pair	-12.1 dB	1.07	1.8 dB	21.61%
MFD Pair with side reflector	-10.6 dB	1.38	3.3 dB	32.29%
MFD Pair with side and top reflectors	-9.46 dB	1.66	4.44 dB	42.20%
Moxon	-10.4 dB	1.21	3.5 dB	24.29%
Moxon with side reflector	-8.18 dB	1.7	5.72 dB	40.14%
Moxon with side and top reflectors	-7.62 dB	1.79	6.28 dB	**47.45**%
Microstrip	-9.72 dB	1.56	4.18 dB	20.20%
Microstrip with side reflector	-7.55 dB	1.7	6.35 dB	18.74%
Microstrip with side and top reflectors	-7.27 dB	1.43	**6.63** dB	20.02%

to road surfaces in particular fall victim to this problem. Operating frequencies and typical deployment geometries are also contributing factors.

We have offered an approach for co-designing the antenna and the roadway-mounted enclosure. This yielded a 6 db improvement in gain using a Moxon Rectangle antenna with the possibility of minimal mechanical impact to the enclosure. A key concept is introducing directivity as a way to improve low elevation angle performance via passive reflectors. This is both a blessing and a curse–a blessing because it is possible to recoup some of the losses from ground reflection, but a curse in that it now falls to the designers of smart city sensors to *exploit* this directivity. Because we can't count on properly aligning each and every sensor with its respective gateway at installation time, sensors must self-adapt by employing software-controllable means to reorient the directivity toward the gateway, wherever that may be.

We have shown that passive reflectors that can be part of the mechanical structure of smart city sensors can be used to further improve low elevation angle performance. We believe that mechanical / RF co-design is both an intriguing and necessary step for smart city sensors. Brinster [18] has explored such co-design using evolutionary algorithms. We believe this is a fruitful direction for smart city sensor RF performance optimization.

VII. Acknowledgements

This work was supported in part by the National USDOT University Transportation Center for Safety for which the authors are grateful. We offer heartfelt thanks to Ervin Teng, João Diogo Falcão, Cef Ramirez, Ritchie Lee and Manal Sinha for their continuous support during this project.

References

[1] B. Iannucci and A. Rowe, "Crowdsourced Smart Cities," in *Intelligent Transportation Society of America (ITS) World Congress*, Montréal, 2017.
[2] S. Mathur, A. Sankar, P. Prasan, and B. Iannucci, "Energy Analysis of LoRaWAN Technology for Traffic Sensing Applications," in *Intelligent Transportation Society of America (ITS) World Congress*, Montréal, 2017.
[3] Semtech, "LoRa Modulation Basics," no. May, pp. 1–26, 2015. [Online]. Available: http://www.semtech.com/images/datasheet/an1200.22.pdf
[4] C. Sommer, S. Joerer, and F. Dressler, "On the Applicability of Two-Ray Path Loss Models for Vehicular Network Simulation," in *Vehicular Networking Conference (VNC), 2012 IEEE*. IEEE, 2012, pp. 64–69.
[5] Voors, Arie, "NEC Based Antenna Modeler and Optimizer," 2015. [Online]. Available: http://www.qsl.net/4nec2/
[6] Dassault Systemes, "CST Studio Suite," 2017. [Online]. Available: https://www.cst.com/products/csts2
[7] L. E. Vogler and J. L. Noble, *Curves of Ground Proximity Loss for Dipole Antennas*. US Department of Commerce, National Bureau of Standards, 1963, vol. 13.
[8] D. B. Miron, *Small Antenna Design*. Newnes, 2006.
[9] D. Liao and K. Sarabandi, "Terminal-to-Terminal Hybrid Full-Wave Simulation of Low-Profile, Electrically-Small, Near-Ground Antennas," *IEEE Transactions on Antennas and Propagation*, vol. 56, no. 3, pp. 806–814, March 2008.
[10] T. L. Roach and J. T. Bernhard, "Investigation of Desired Element Pattern Reconfigurability in Small Adaptive Arrays," *IEEE Transactions on Antennas and Propagation*, vol. 64, no. 12, pp. 5441–5446, Dec 2016.
[11] O. Kramer, T. Djerafi, and K. Wu, "Vertically Multilayer-Stacked Yagi Antenna With Single and Dual Polarizations," *IEEE Transactions on Antennas and Propagation*, vol. 58, no. 4, pp. 1022–1030, April 2010.
[12] W. Liang, Y. Qi, and Y. C. Jiao, "A Novel Small Director Array for Slot Loop Antenna for LTE Application," *IEEE Antennas and Wireless Propagation Letters*, vol. 12, pp. 1110–1113, 2013.
[13] H. A. Wheeler, "Fundamental Limitations of Small Antennas," *Proceedings of the IRE*, vol. 35, no. 12, pp. 1479–1484, Dec 1947.
[14] A. Haskou, S. Collardey, and A. Sharaiha, "Small Array Design using Parasitic Superdirective Antennas," in *2016 10th European Conference on Antennas and Propagation (EuCAP)*, April 2016, pp. 1–4.

[15] R. Marg, I. Schön, and A. Jacob, "Finite Ground Plane Effects on the Radiation Pattern of Small Microstrip Arrays," *IEE Proceedings-Microwaves, Antennas and Propagation*, vol. 147, no. 2, pp. 139–143, 2000.
[16] C. A. Balanis, "Antenna Theory," 2012.
[17] Y. Choi, U. Kim, J. Kim, and J. Choi, "Design of Modified Folded Dipole Antenna for UHF RFID Tag," *Electronics Letters*, vol. 45, no. 8, pp. 387–388, 2009. [Online]. Available: isi:000265234100003
[18] I. Brinster, "Multi-objective Algorithms for Coupled Optimization of Mechanical and Electromagnetic Systems," *CMU Department of Electrical and Computer Engineering*, vol. 492, Ph.D. dissertation, 2014. [Online]. Available: http://repository.cmu.edu/dissertations/492

VIII. Appendix

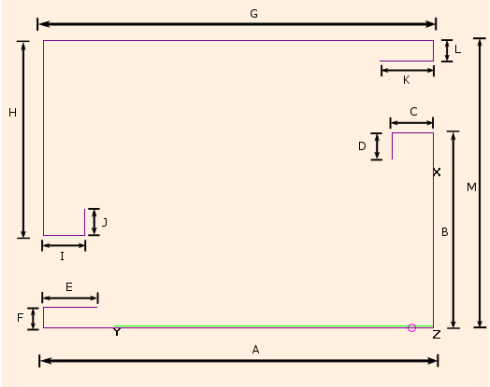

Fig. 14: MFD Pair

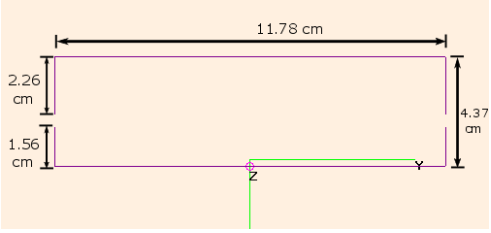

Fig. 15: Moxon

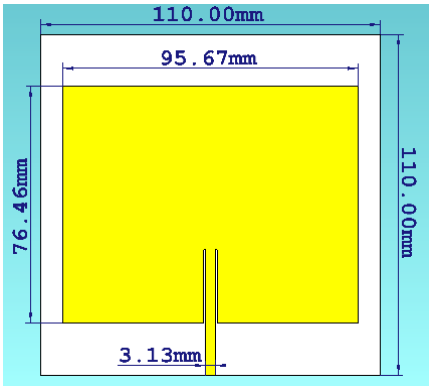

Fig. 16: Microstrip patch antenna modeled on a 1.6mm FR4 substrate with a copper pour on the back side. The thickness of the conductor is 0.035mm.

TABLE III: Reflector dimensions with respect to the antennas

Dimension	MFD Pair	Moxon	Patch
H1	0.1 cm	0.6 cm	0.4 cm
L1	0.5 cm	0.35 cm	0.3674 cm
H2	0.8195 cm	1.262 cm	1.3674 cm
L2	1.0927 cm	1.35 cm	0.95 cm
W	1.7018 cm	1.7018 cm	1.7018 cm
L	11.938 cm	11.938 cm	11.9 cm
O	2.69064 cm	0.158 cm	0.45 cm

TABLE IV: MFD Pair dimensions for shrinking antenna sizes. Antenna pair with spacing of 11 cm is the one used with reflectors.

Spacing (M)	11 cm	10 cm	9 cm	8 cm	7.5 cm
A/B/G/H	6.09 cm	6.09 cm	6.09 cm	6.09 cm	6.09 cm
I/C/F/L	1.54 cm	1.09 cm	0.603 cm	1.4 cm	0.8 cm
D/E/J/K	0.84 cm	0.84 cm	0.84 cm	0.84 cm	0.84 cm

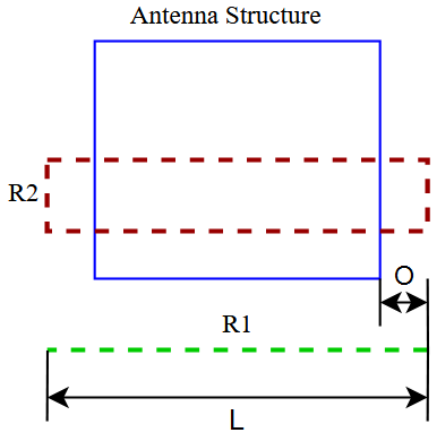

Fig. 17: Top view of the reflector setup

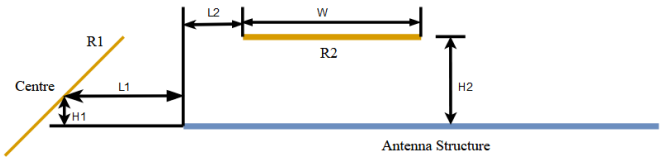

Fig. 18: Side view of the reflector setup. The vertical distances are given with respect to the geometric centers of the components.